TN051: Test beam proton calorimetry note

Josh Devan

July 17, 2014

Abstract

This note describes the derivation of a systematic error on the calorimetric response of protons in the MINERνA detector from a comparison of data and MC in the test beam detector in both the T/E and E/H configurations. The test beam detector saw protons of 50 MeV to 1.5 GeV kinetic energy (Figure 1). A data/MC ratio of the mean calorimetric response over kinetic energy (Figure 7) shows agreement within systematic errors. The final uncertainty on the calorimetric response of protons is taken as the systematic error, 3.0% at higher energies. The uncertainty can be expanded to 3.5% at 100 MeV KE and 4.0% at 50 MeV.

1 Test beam

The test beam detector consists of 40 scintillator planes of $\sim$1 m^2 active area (63 $\sim$1 m strips). The planes can be interleaved with sheets of 2 mm lead and 1 in steel to emulate the downstream calorimeters of the MINERνA detector. During the Summer of 2010, we ran two configurations: T/E (20 tracker modules upstream, 20 ECAL modules downstream) and E/H (20 ECAL modules upstream, 20 HCAL modules downstream). Other than dimensions, the test beam detector readout system differs from MINERνA in only one way: the test beam detector does not use clear fiber; the WLS fiber plugs directly into the PMT's.

A tertiary beamline produces, identifies and momentum-analyzes particles entering the test beam detector. With the beamline selecting positively charged particles, the detector saw protons from 50 MeV to 1.5 GeV kinetic energy (see Figure 1). A data-driven MC sample is generated by feeding the position and momentum vectors of particles immediately upstream of the third wire chamber into the simulation. The simulation propagates particles through the aluminum windows of the two downstream wire chambers, the downstream time of flight (TOF) scintillator, the muon trigger scintillator and the air in the experiment hall before impacting the test beam detector. The seeded magnitude and direction of the momentum vector is smeared according to a Kalman filter prediction as described in TN017, docdb:8547. TN017 also describes the uncertainty on the momentum measurement from the beamline.

The tertiary beamline produces particles to impact the detector by colliding secondary 16 GeV pions on a copper target. We are measuring single particle response and thus want a single particle to impact the detector per readout gate. Pile-up, however, is introduced from multiple particle production by a single pion, pions in adjacent accelerator buckets with a $\pm n\times$19 ns separation and muons from pion decays upstream of the target.

2 Event selection

The event sample is required to pass the following cuts:

1. **Loose beamline quality** – The beamline reconstruction software (MTestBeamReco) identifies events passing a set of "loose" and/or "strict" quality cuts. These cuts require a particle

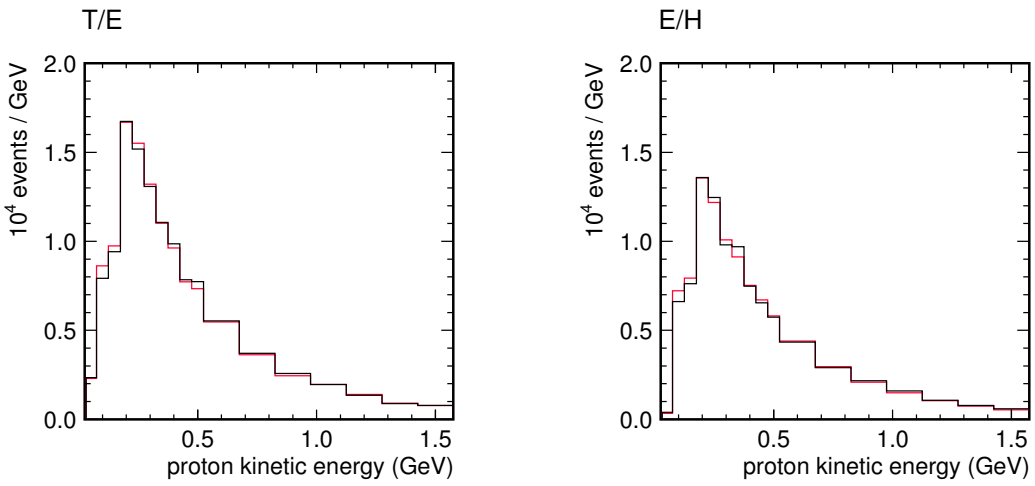

Figure 1: Event rate after all selection cuts vs. proton kinetic energy. Data in black; MC in red. MC area normalized to data. MC is 20× statistics.

track through all four wire chambers, a valid momentum fit with a trajectory that doesn't stray too much into the poorly simulated regions of the magnetic field, a valid TOF measurement and for the strict cuts, a maximum fit χ^2. The loose cuts are implemented by default. As a systematic study, the strict cuts are also included.

2. **Beamline identified proton** – The beamline reconstruction software sets a particle identification code based on a combination of mass and TOF cuts. Protons are identified by a calculated mass within ±20% of 938.3 MeV.
3. **Clean beamline to detector match** – TBCleanEventTool performs a beamline to detector matching algorithm by projecting from the beamline measured particle trajectory to the face of the detector. The algorithm verifies the presence of scintillator activity at this point and the absence of activity away which indicates a stray particle entered the detector.
4. **No adjacent time slice within 250 ns before and 500 ns after the primary proton** – Particle showers from upstream interactions can cause a number of time slices to be generated adjacent to each other. This can produce a number of technical problems, such as dead time, the wrong slice identified as the proton or even tracks separated into separate time slices by the ChronoBuncher. It is also observed that when time slices are spaced closely together, the primary slice is more likely to have pile-up background.
5. **TOF not within 19 ns shadow region** – As an artifact of the 19 ns separation of adjacent accelerator buckets, the TOF spectrum is shadowed at +19 ns (see Figure 2). Events between 38.0 and 41.0 ns, which are potentially mis-identified pions, are rejected.
6. **Background vetoes** – In the lower energy bins, where the proton is expected to be well contained in the upstream portion of the detector, downstream modules are utilized as background vetoes. Events are rejected with significant visible energy in these modules which is likely the result of beam backgrounds, such as muons. The details of this are explained in Section 3.
7. **Absurd calorimetric reconstruction** – Events are rejected for which the ratio of the calorimetric response to proton kinetic energy is greater than 2.0. In the MC, such events are nearly non-existent. In the data, it is evident of a background particle interaction in the detector.

Events passing cuts 1, 3 and 4 above are identified with the flag "PassAll", set by MTestDataAlg. PassAll and the particle identification code (PDG code), also set by MTestDataAlg, form the basis of any selection for test beam analyses.

The proton event sample passing these cuts is displayed in Figure 1.

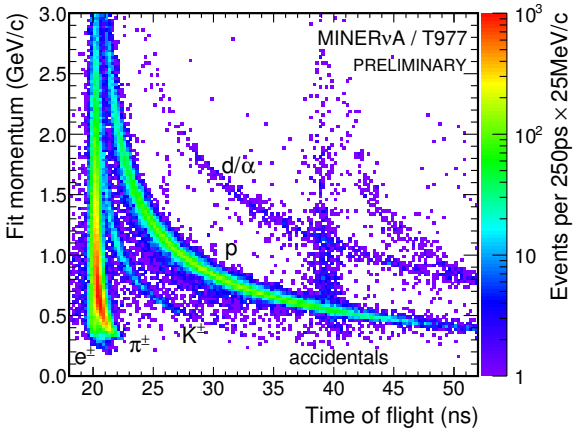

Figure 2: Momentum vs. time of flight for all particles in the Summer 2010 test beam run. Nearly speed of light particles peak at ∼20 ns from the ∼6 m path length in the beamline. The spectrum is shadowed at +19 ns from events in which a particle triggers the upstream TOF scintillator, but a second particle in the next accelerator bucket triggers the downstream TOF.

3 Calorimetry

The calorimetric response is defined as:

$$\text{calorimetric energy} \equiv \sum_i c_i E_i \tag{1}$$

$$c_{TRAK} = 1.26 \tag{2}$$

$$c_{ECAL} = 2.08 \tag{3}$$

$$c_{HCAL} = 10.73 \tag{4}$$

The sub-detector constants, c_i, are calculated from the dE/dx of a minimum ionizing particle at normal incidence and include the active fraction of a scintillator plane. The summation is over all clusters in the time slice identified as the proton, regardless of timing or type. In big MINERνA, we impose a narrow time window on the included clusters, within 20 ns before and 35 ns after the interaction vertex time and reject clusters identified as cross-talk to remove energy from the muon.

The data has backgrounds from three sources: muons from pion decays in the secondary pion beam, pions from interactions in the target of our tertiary beamline and a persistent flux of low energy neutrons from interactions in the target, detector and hall. The muon and pion background can be rejected by identifying a secondary particle entering the front of the detector (as performed in the third cut of the event selection) and identifying a highly penetrating particle, uncharacteristic of a proton.

The neutron flux is more difficult to reject. An observation of energy in the time slice much earlier than the proton interaction sets the magnitude of the neutron flux as a few MeV per event, calorimetrically weighted. In the lowest kinetic energy bin of 100 MeV, this amounts to a few percent

correction, which is severe on what is to be a few percent measurement. To mitigate the effects, the following scheme is implemented:

In the lowest kinetic energy bins, $\leq$ 150 MeV (T/E) 200 MeV (E/H), only the upstream sub-detector is integrated calorimetrically because the proton is well contained upstream at those energies. The downstream sub-detector is utilized as a muon/pion veto, rejecting events with greater than 10.0 MeV summed visible energy.

For higher energy, $\leq$ 300 MeV (T/E) 750 MeV (E/H), the entire detector is integrated. The last four planes are utilized as a muon/pion veto, rejecting events with greater than 2.0 MeV summed visible energy. This scheme follows what was performed in the pion calorimetry analysis, TN045, docdb:9474.

For the highest energy bins, the entire detector is integrated and no veto is incorporated.

The magnitude of the effect of including this scheme is shown in Figure 23.

The analysis is performed by histogramming the calorimetric response for data and MC in bins of proton kinetic energy. Figure 3 shows the calorimetric energy and calorimetric energy ratio to kinetic energy for the 200 MeV bin of the T/E detector. The mean and RMS of this distribution quantify the agreement of data and MC and are summarized in the plots in Section 4.

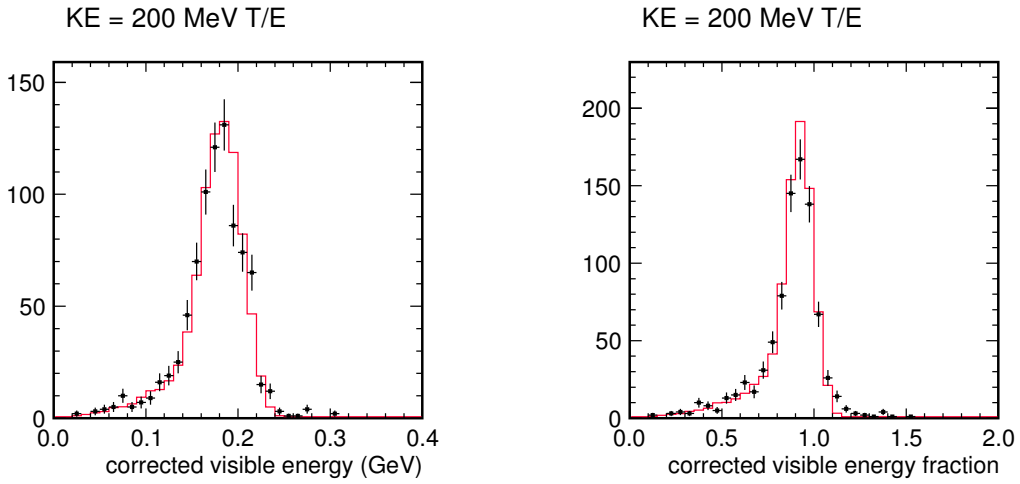

Figure 3: **Left:** Calorimetric energy for the 200 MeV kinetic energy bin in the T/E detector. **Right:** Calorimetric energy / KE for the same bin. Data in black with statistical errors; MC in red.

4 Results

Figure 4 displays the mean of the calorimetric response (see example, left of Figure 3) vs. proton kinetic energy. The left most bin is hatched out because of poor statistics. The bins on the right are hatched because the proton is poorly contained, penetrating through the back of the detector.

Figure 5 displays the mean of the calorimetric response divided by proton kinetic energy (see example, right of Figure 3) vs. proton kinetic energy. The RMS of the same distribution is plotted in Figure 6. A data/MC ratio of the means is plotted in Figure 7, which is the primary result of the analysis.

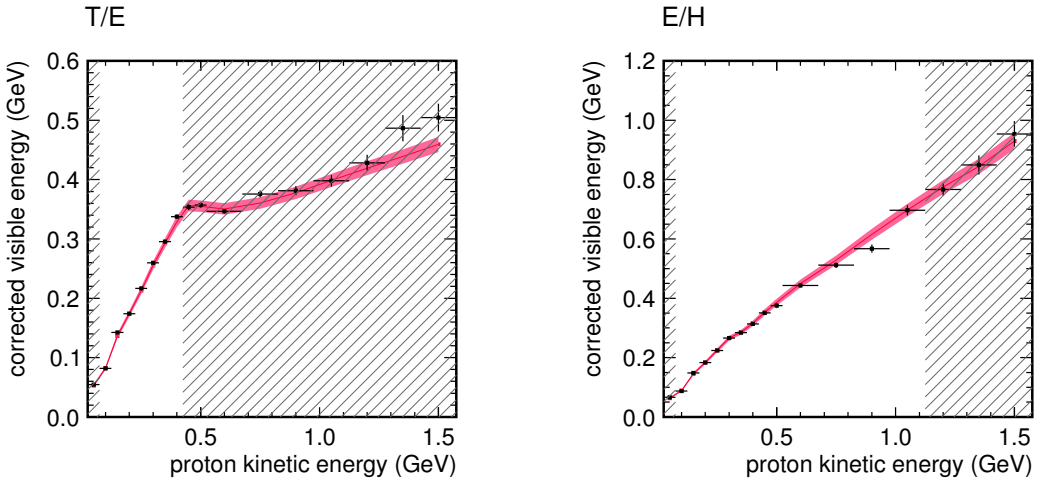

Figure 4: Mean of calorimetric energy vs. proton kinetic energy. Data in black with statistical errors. MC in red with systematic errors.

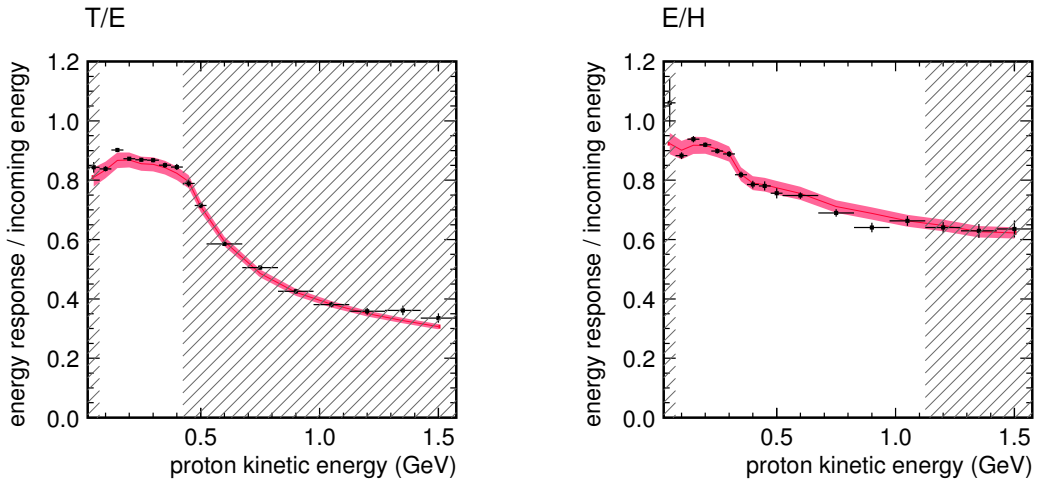

Figure 5: Mean of calorimetric energy / KE vs. proton kinetic energy. Data in black with statistical errors. MC in red with systematic errors.

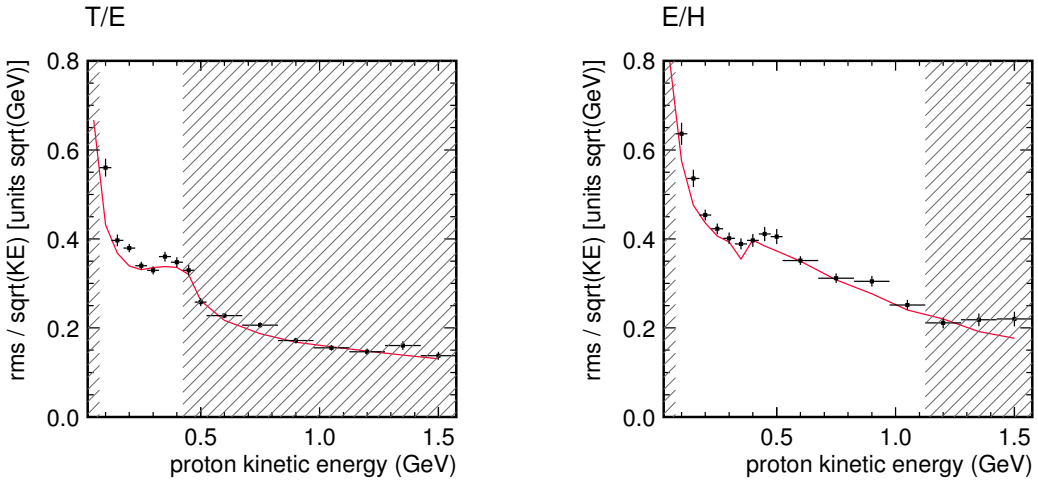

Figure 6: RMS of calorimetric energy / KE vs. proton kinetic energy. Data in black with statistical errors; MC in red.

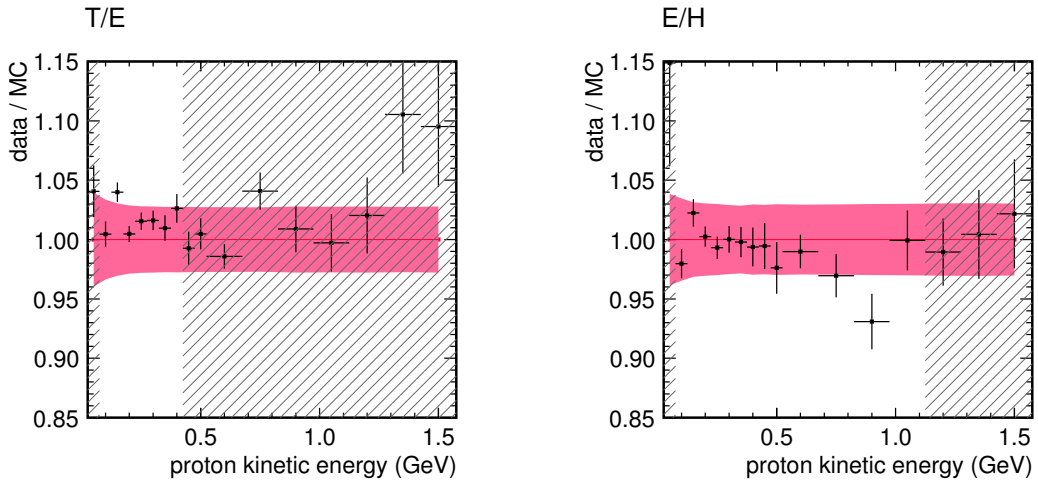

Figure 7: Data/MC ratio of Figure 5 (mean of calorimetric energy / KE vs. proton kinetic energy). Data in black with statistical errors. MC in red with systematic errors.

5 Systematic errors

5.1 Calibration and energy scale

The test beam detector calibration is described in tech note TN018, docdb:8686.

5.1.1 MEU/LY

The energy scale calibration procedure produces two constants: MEU (muon equivalent unit) and LY (light yield). LY converts from photons to photoelectrons (PE) in the MC, by matching the photoelectrons observed in the data. MEU converts from PE to MeV, by matching the MC truth energy deposited in the active scintillator of the detector planes. The calibration is performed with through-going muons depositing MIP-scale energies.

TN018 gives the uncertainty on the energy scale arising from the MEU/LY tuning as 1.1% on the absolute scale and 0.6% on data/MC comparisons. The dominant components of the uncertainty are the intrinsic uncertainty of the polynomial fit to the energy distributions and an unexplained difference in the MEU factor between the T/E and E/H detectors.

5.1.2 Cross-talk

A measurement of the cross-talk in data finds an average of $4.2 \pm 0.5\%$ over the first 25 planes. The cross-talk in MC is scaled to this value. The MEU calibration, however, only considers energy deposited on the muon track and thus is tuning $100 - 4.2\% = 95.8\%$ of the PE to 100% of the true deposited MeV. This results in the absolute energy scale being high by 4.2%. For this and other calorimetry analyses, the absolute response of data and MC is scaled down by this value.

5.1.3 LPos effect

The LPos (longitudinal position) effect is a position-dependent calibration discrepancy between the data and MC. In the data, it is observed that (after attenuation correction), the calibrated energy varies across the length of a strip. The final cause was never determined; an incorrect measurement or application of attenuation is a possibility (TN018 describes the problem in greater detail). The kludge tool, WilliamClayFordSystematicsTool, provides a means of generating a shifted MC sample including the LPos effect observed in data. Figure 8 shows the ratio of shifted to unshifted energy response / incoming energy versus proton KE. The effect is 0.3% at 100 MeV, becoming even more negligible at high energy. It is included in the error band as energy-dependent.

5.1.4 PMT non-linearity

PMT non-linearity is not currently modeled in the MC, but TBAna includes code to compute a 2σ correction based on a calculation by Howard Budd (details in TN018). Figure 9 shows the ratio of shifted (with non-linearity) to unshifted (without non-linearity, the default) MC. The 1σ effect is 0.7% constant across energy. While this is actually a one-sided uncertainty (non-linearity can only decrease the energy response), it is incorporated symmetrically.

PMT non-linearity is evaluated here for a single proton, but could potentially be a more significant uncertainty in the big detector for multi-particle final states and large EM showers. The effect should be included in the systematic error on the calorimetric reconstruction of the recoil system.

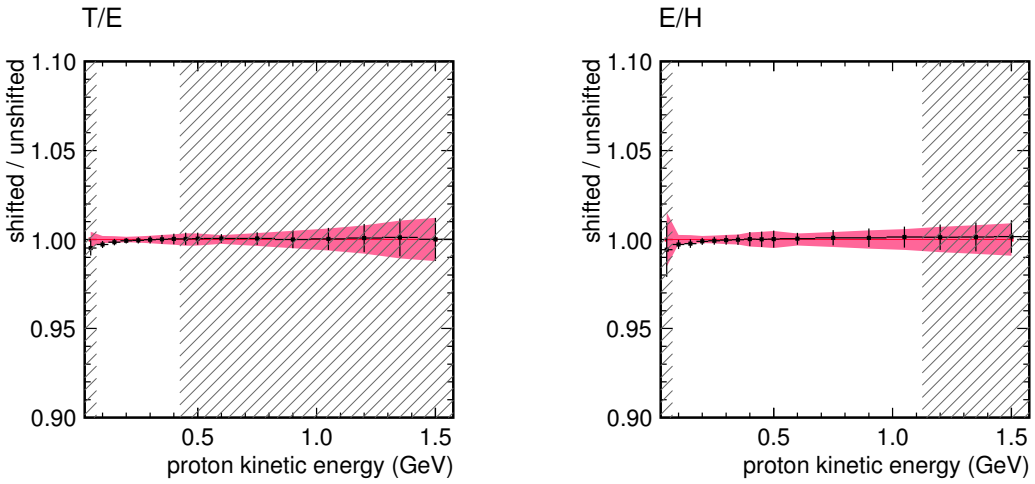

Figure 8: LPos effect; a residual position-dependent calibration error observed only in the data.[1]

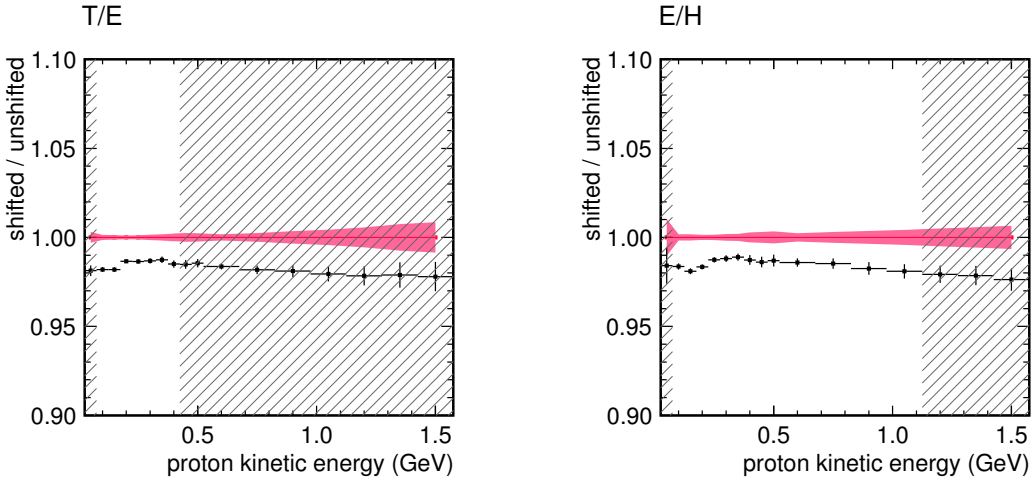

Figure 9: PMT non-linearity (2σ).[1]

5.1.5 Birks' constant

Birks' constant and uncertainty are determined by Rik's stopping proton analysis (see TN037, docdb:9131). Figures 10 and 11 show the ratio of shifted to unshifted MC for $\pm 15\%(1\sigma)$ variations. The effect is 2.3% at 100 MeV and 1.2% (T/E) 1.5% (E/H) at higher KE. A change to Birks' constant affects the MEU tuning, should the full calibrations be re-performed. For a 15% shift in Birks' constant, the MEU shifts by 0.3%. This component of the uncertainty is already included with the MEU and is subtracted from the energy-dependent Birks' uncertainty, yielding a final uncertainty of 2.0% at 100 MeV and 0.9% (T/E) 1.2% (E/H) at higher KE.

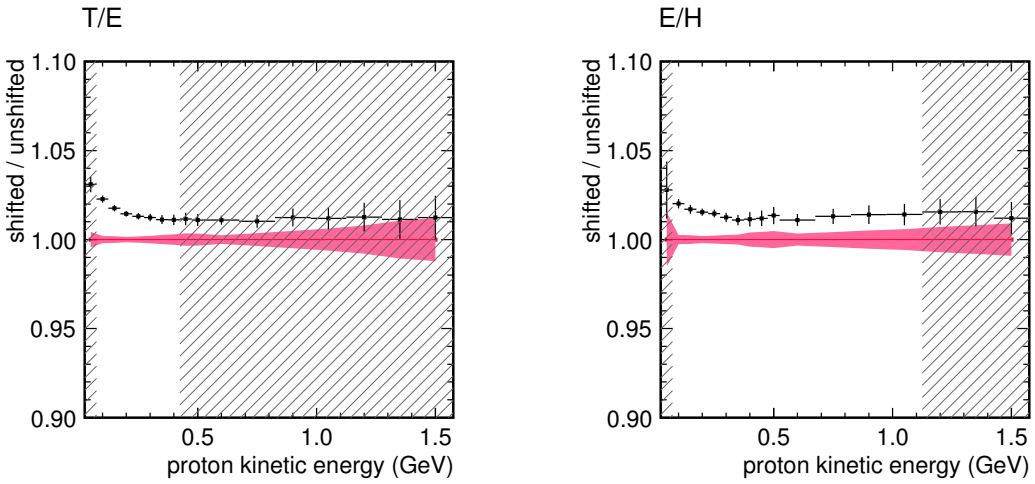

Figure 10: Birks' constant -15%.[1]

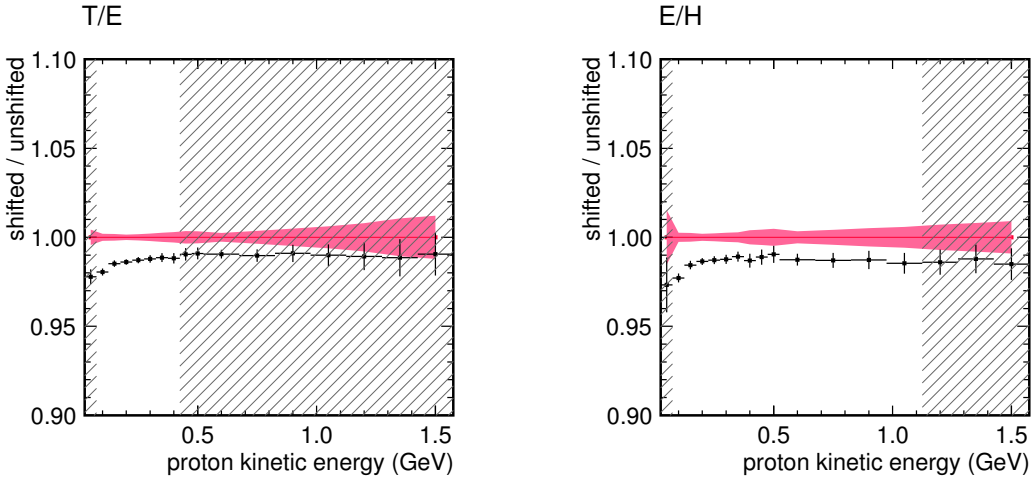

Figure 11: Birks' constant $+15\%$.[1]

[1]Statistical errors ($\sqrt{n}$) for the unshifted MC are plotted in red; for the shifted MC are plotted in black on the ratio. But these are identical Geant-simulated events (the shift is applied during calibration), so the error is effectively zero.

5.2 Mass model

The uncertainty on the scintillator plane mass model has two components: the total amount of material and the active fraction. The uncertainty on the total material in a scintillator plane is 1.5%. The uncertainty on the active fraction is much larger at 3–5% and has not been well evaluated. For a calorimetry analysis, however, the active fraction cancels out and we can take the smaller 1.5% uncertainty.

The argument (interpreted from TN018) is that through the LY tuning, the PE in the MC is matched to that in the data. The MEU is then set to convert from this PE to the MC truth energy deposited in the active part of the scintillator plane, which is effectively the active fraction times the total deposition in the plane. For calorimetry, we correct to the total deposition in the plane by dividing by the active fraction. There is a small effect from different photostatistics, but the dominant uncertainty is on the energy deposited in an entire plane by a through going muon, which is given by the total material uncertainty.

Figures 12, 13 and 14 show the ratio of shifted to unshifted MC for 2σ variations in the lead and iron of the ECAL and HCAL sub-detectors. The 1σ uncertainty from the lead mass is taken as 0.2% for the T/E detector in the 300 MeV bin and above and 0.4% constant for the E/H detector. The 1σ uncertainty from the iron mass is taken as 0.4% for the E/H detector in the 400 MeV bin and above.

Figure 15 shows the ratio of shifted to unshifted MC for a 2σ variation in the thickness of the aluminum foils in the wire chambers of the tertiary beamline. The 1σ effect is 0.7% at 100 MeV. It is implemented as an energy-dependent systematic with a value of 0.7% at 100 MeV, linearly falling to zero at 300 MeV.

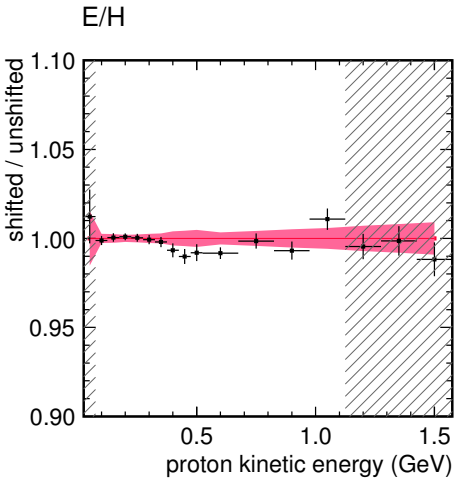

Figure 12: Fe density +2.0% (2σ).

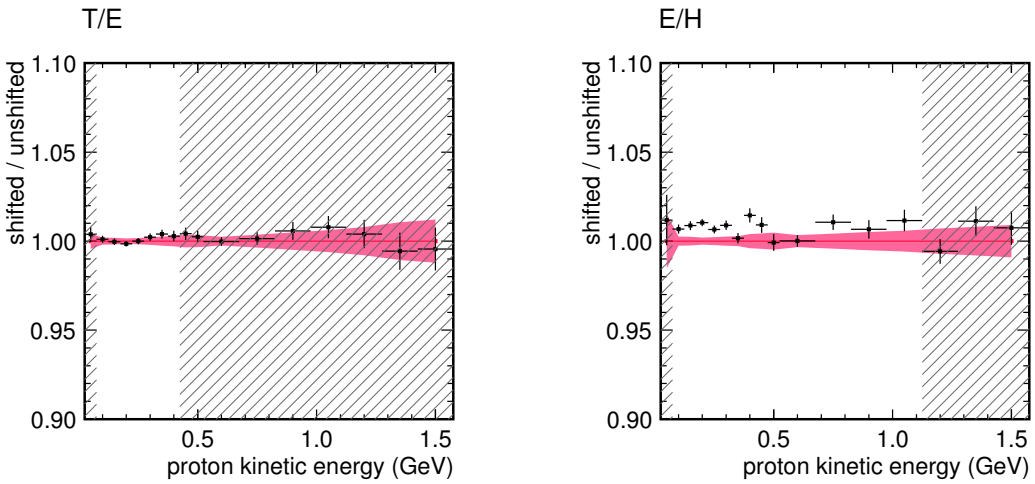

Figure 13: Pb density -2.4% (2σ).

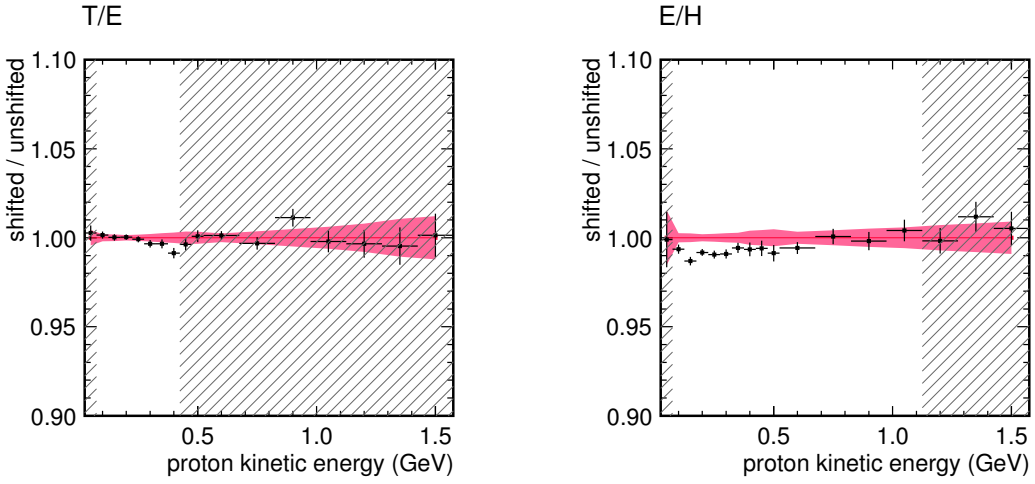

Figure 14: Pb density $+2.4\%$ (2σ).

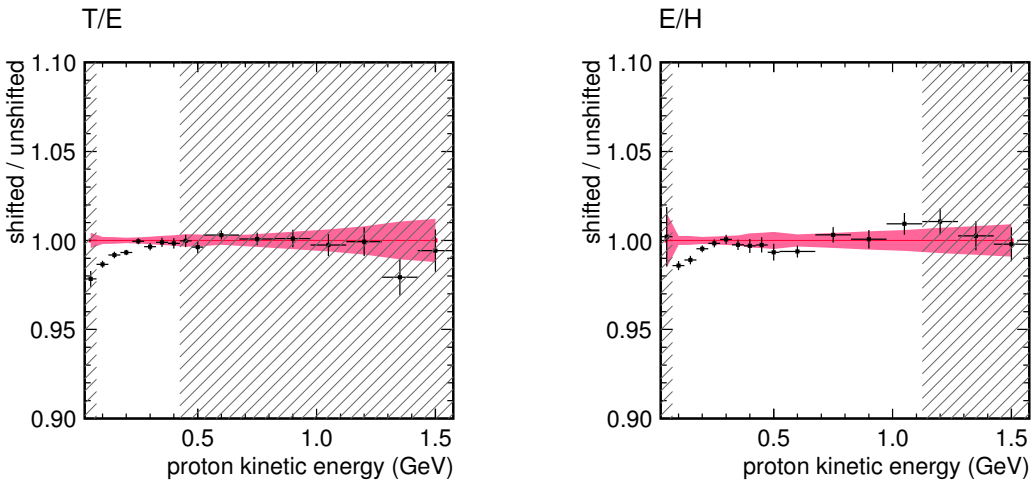

Figure 15: Thickness of wire chamber aluminum foils +400% (2σ).

5.3 Beamline momentum

The beamline resolution and systematic errors are documented in TN017, docdb:8547.

The uncertainty on the beamline momentum has four components: a momentum-dependent alignment uncertainty of 1.0% per GeV/c (i.e. 0.5% at 500 MeV/c, 1.0% at 1 GeV/c) and three constant magnetic field uncertainties of 0.5%. The four are added in quadrature to form the final momentum uncertainty. Figures 16 and 17 show the ratio of shifted to unshifted MC for a positive and negative shift in beamline momentum. The uncertainty is taken as 1.9% constant.

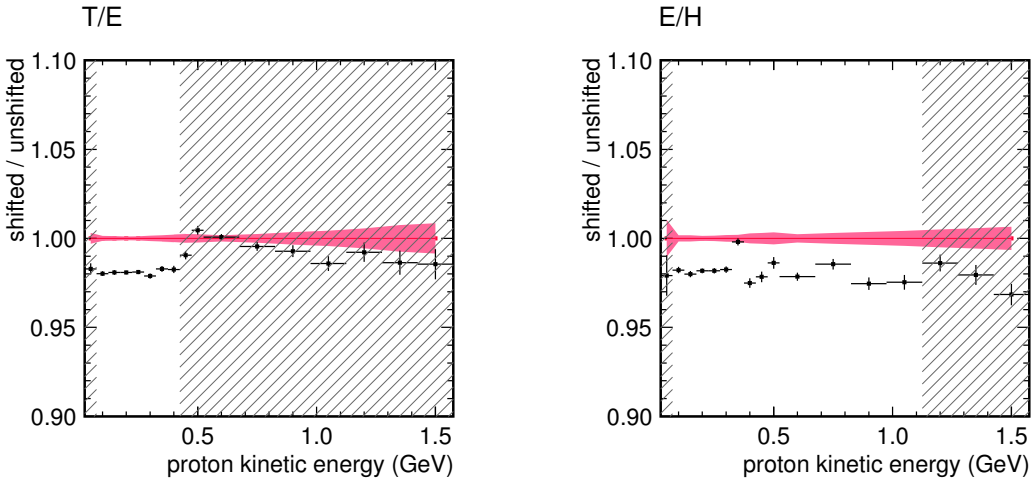

Figure 16: Beamline momentum shifted up.

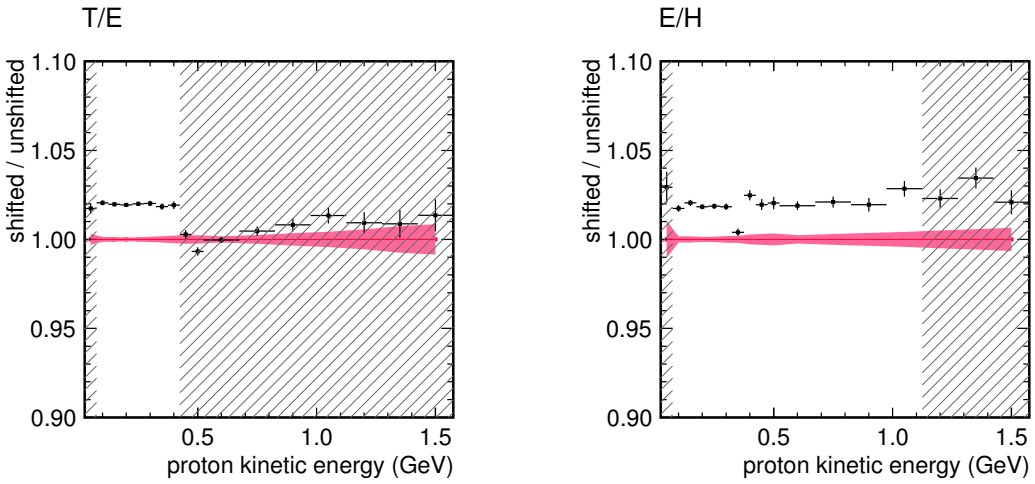

Figure 17: Beamline momentum shifted down.

5.4 Stability

The temperature in the experiment hall varied wildly during the Summer 2010 run due to a failed HVAC unit. The temperature was lowest at 4 AM for the start of data taking and highest at 6 PM when beam was disabled. The average hall temperature rose as the run proceeded later into Summer. A correction was implemented as described in TN018. The correction uses the temperature probe located near the test beam detector and connected to ACNET to correct the approximately -0.4% per degree Celsius degradation in energy reponse with rising temperature.

Figure 18 shows the stability of the data after this correction through the ratio of high temperature data (> 28 C) to low temperature data (< 28 C). No distinguishable trend is observed, so no additional systematic uncertainty is included.

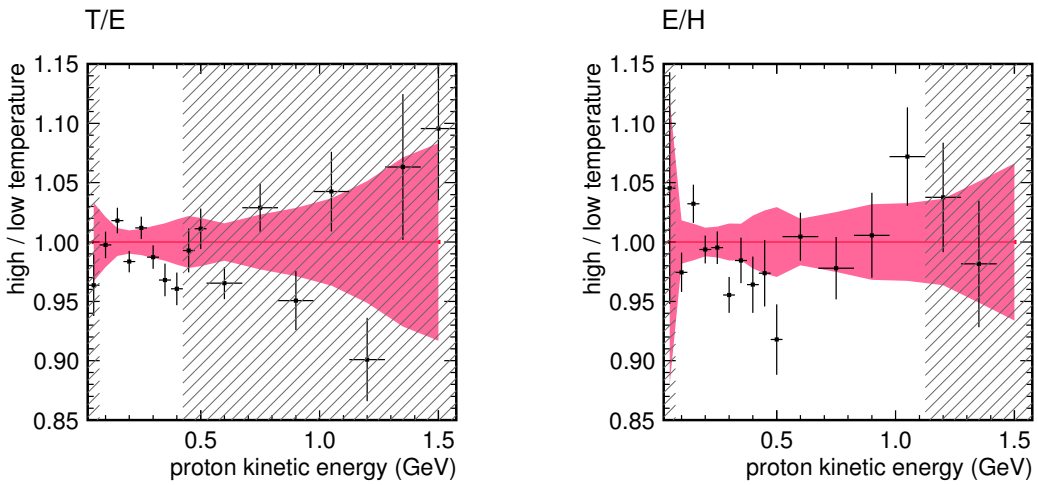

Figure 18: Temperature stability.

Figure 19 divides the data set by vertical position at the most downstream wire chamber (WC4). Again, no trend is observed. The equivalent plot for horizontal position is not utilized because horizontal position is correlated with particle momentum.

Figure 20 divides the data set by time, plotting the ratio of the first and second half of the T/E and E/H runs. No trend is observed.

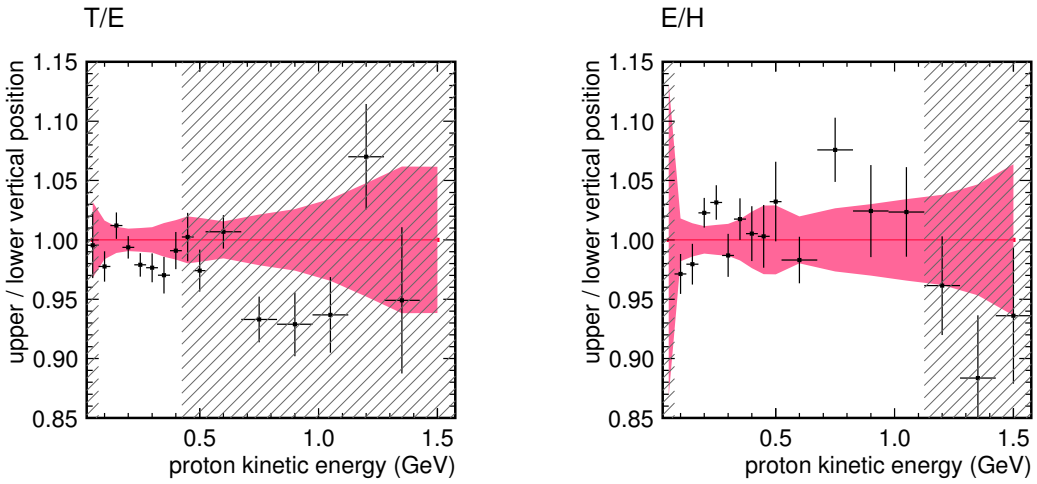

Figure 19: Vertical position stability.

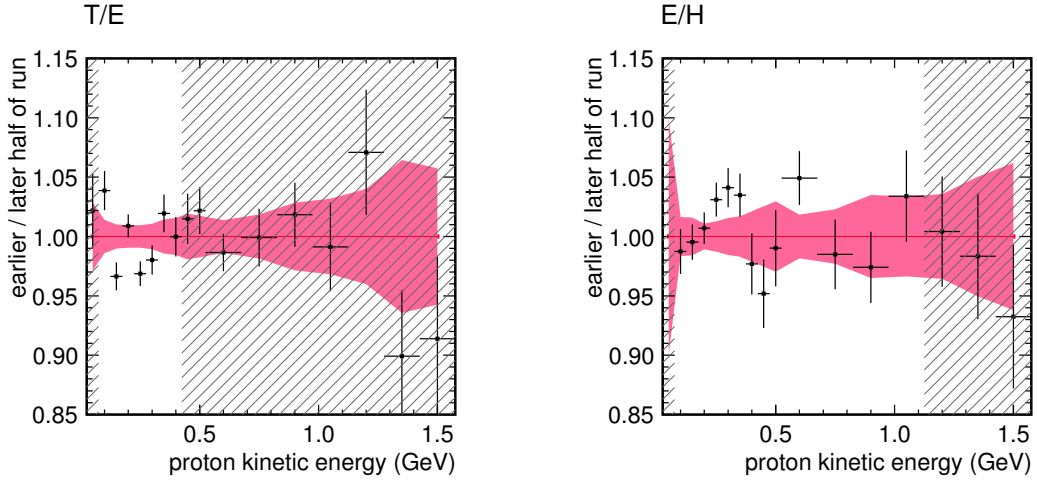

Figure 20: Time stability.

5.5 Event selection

The default beamline selection is the "loose" beamline cuts; as a systematic study, we implement the "strict" cuts, which includes additional limits on the magnetic field integral, the magnetic error integral (the magnetic error is non-zero in the more questionable regions of the field) and the fit χ^2. Figure 21 is a double ratio of data/MC energy response / incoming energy of the strict cuts over the default cuts. The strict cuts are not expected to affect the MC in any way other than varying the momentum distribution of protons. As evidenced in the plot, the data is not affected either.

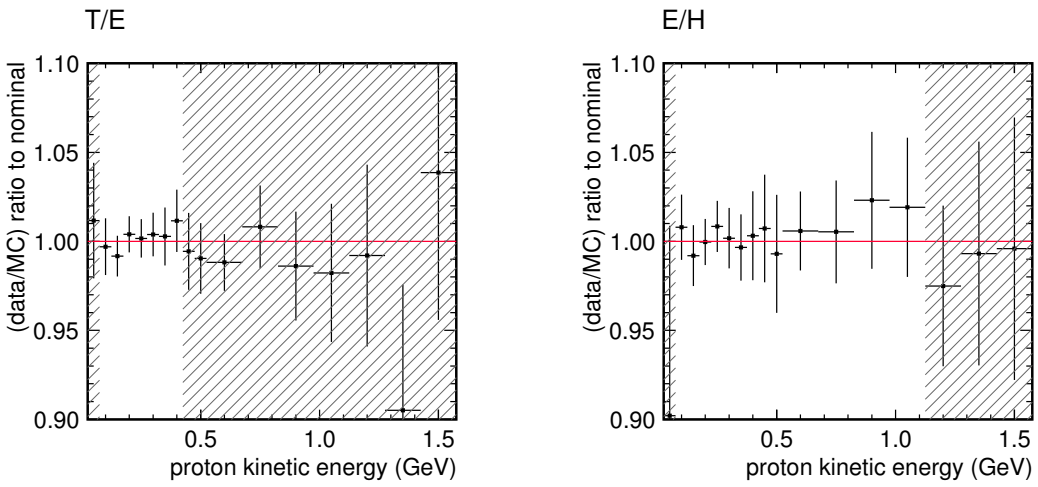

Figure 21: Strict beamline quality cuts.

The default beamline selection cuts events with an adjacent time slice less than 400 ns before or 200 ns after the primary slice. This removes events with dead time from earlier activity and events that are part of large cascades from an upstream shower that generate many time slices. The time window is doubled to 800 ns before or 400 ns after as a systematic study, shown in Figure 22. The effect is 0.3% in the T/E detector and 0.6% in the E/H detector, taken as a constant.

The origin of this systematic is not immediately clear; adjacent time slices can be caused by beam backgrounds (only in the data), PMT after-pulsing, late neutron hits, Michel electrons and other decay products.

5.6 Pile-up background

The default analysis ignores the downstream sub-detector for the very low energy events to avoid integrating the background of neutrons drifting through the hall from upstream interactions. The downstream sub-detector is utilized as a veto for these events to remove muon and pion contamination. For mid-energy events, the last four planes are used a muon/pion veto. Figure 23 shows the result of disabling these features of the analysis. This is not taken as a systematic, only an illustration of magnitude.

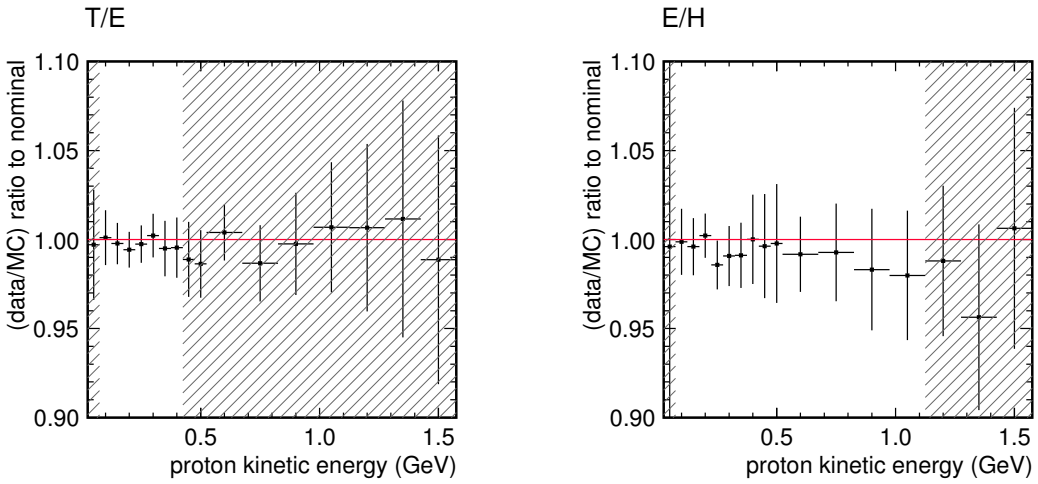

Figure 22: Cut events with an adjacent time slice within $(-800, 400)$ ns ($2 \times$ default window).

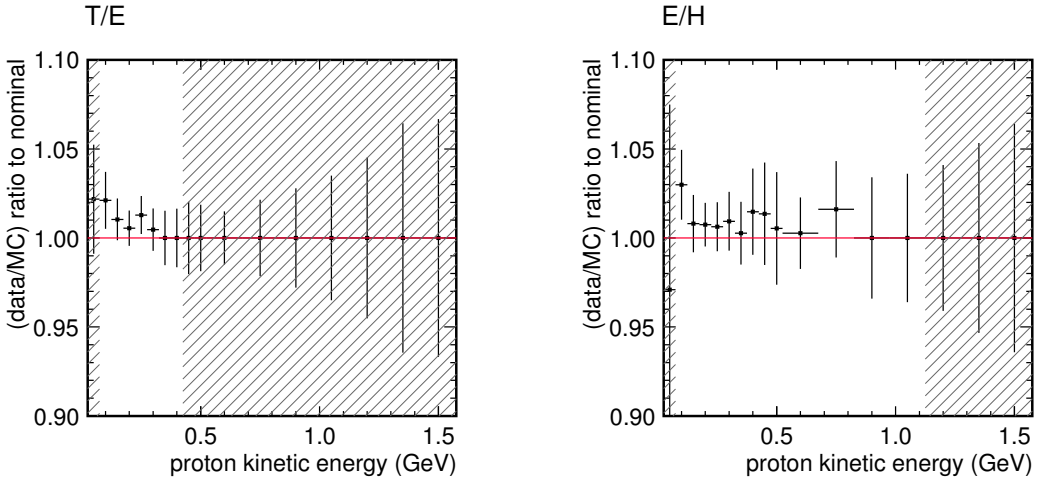

Figure 23: Disable ignoring the downstream sub-detector for low energy events and the pile-up background veto.

5.7 Calorimetry

Figure 24 shows the results of ignoring clusters with energy less than 0.5 MeV in the calorimetric sum. The effect is 0.7% in the T/E detector and 0.9% in the E/H detector, constant in energy. A component of the sub 0.5 MeV clusters is clearly cross-talk. TN018 specifies a cross-talk systematic of 0.5%, but for this analysis, the systematic is expanded to 0.7% and 0.9% to cover all low energy response.

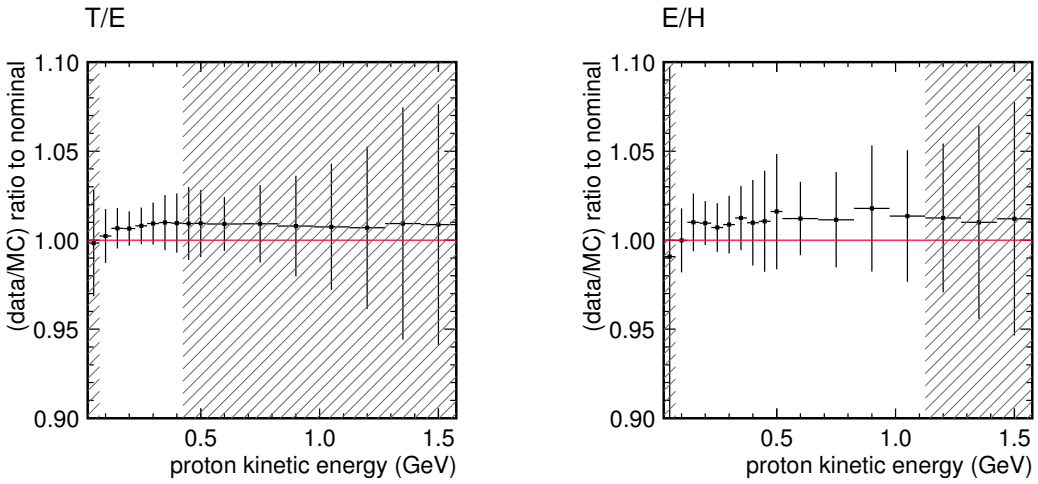

Figure 24: Ignore clusters < 0.5 MeV for calorimetry.

For the reconstruction of the recoil system in the CC inclusive analysis in the big detector, only clusters within a $(-20, 35)$ ns window around the vertex time are included. Figure 25 imposes that same cut on the proton calorimetry analysis. The effect is 1.2% (T/E) and 1.7% (E/H). This is not included in the systematic error for this analysis, but the magnitude indicates it should be considered as part of the systematic error for the recoil system in the big detector.

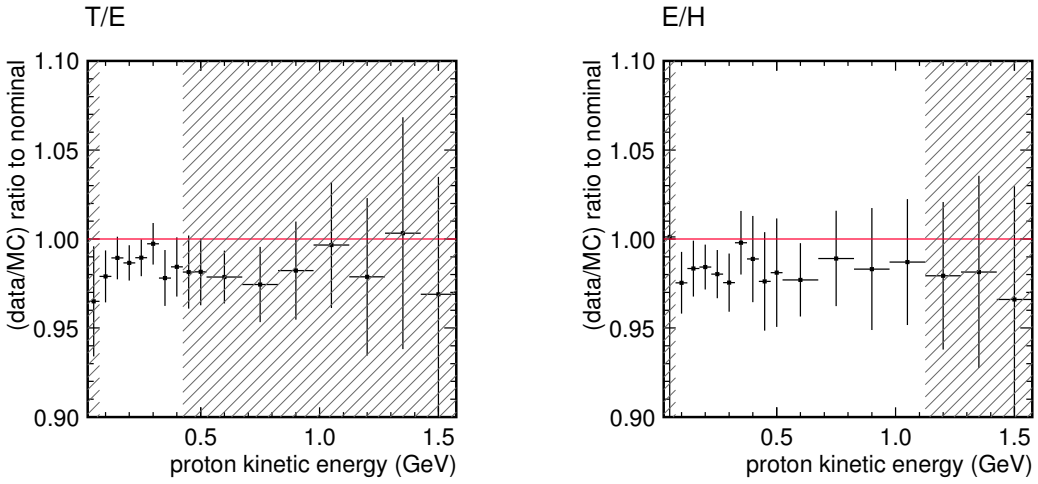

Figure 25: Big detector calorimetry time window (include only clusters within $(-20, 35)$ ns).

5.8 Summary

The systematic errors on the data/MC ratio of energy response / incoming energy are summarized in Table 1.

error	T/E	E/H
MEU/LY	0.6%	0.6%
cross-talk	0.7%	0.9%
LPos	0.3% (100 MeV)	0.3% (100 MeV)
PMT non-linearity	0.7%	0.7%
Birks' constant	2.0% (100 MeV) 0.9% (400 MeV)	2.0% (100 MeV) 1.2% (1 GeV)
scintillator mass	1.5%	1.5%
lead mass	0.2% ($\geq$ 300 MeV)	0.4%
iron mass	N/A	0.4% ($\geq$ 400 MeV)
WC Al foil mass	0.7% (100 MeV)	0.7% (100 MeV)
beamline momentum	1.9%	1.9%
adjacent time slices	0.3%	0.6%
quadrature sum	3.4% (100 MeV) 2.8% (400 MeV)	3.5% (100 MeV) 3.0% (1 GeV)

Table 1: Summary of systematic errors.

6 Eroica vs. Resurrection

The WilliamClayFord MC, used for this and all other test beam analyses, differs from the Resurrection and Titan releases in four ways:

1. **Birks' constant** – Birks' constant is tuned to data, documented in TN037, docdb:9131. The constant is reduced, resulting in an increase in visible light.
2. **Geometry** – The geometry is tuned to the material assessment.
3. **Hit aggregation** – The hit aggregation algorithm, which joins small MC hits into larger ones, is disabled. The algorithm does not respect Birks' suppression, changing the dE/dx profile of the hit. The algorithm will be enabled, but corrected, for future software releases.
4. **Geant neutron settings** – A bug in the Geant settings is corrected which resulted in a failure to simulate low energy neutrons.

These four changes have been proposed for the Eroica software release; the test beam MC is a prototype of Eroica MC. Figure 26 shows the ratio of the mean calorimetric energy / KE vs. proton kinetic energy for Resurrection-era MC over the default test beam, proto-Eroica MC. The effect is nearly 5% constant for protons, a higher calorimetric response in proto-Eroica, mostly from the change in Birks' constant.

The ratio of mean calorimetric energy / KE for Resurrection-era Birks' constant over the new proto-Eroica is shown in Figure 27, for Resurrection-era geometry over proto-Eroica in Figure 28, for Resurrection-era hit aggregation over hit aggregation disabled in Figure 29 and for Resurrection-era hit aggregation and neutron settings over proto-Eroica in Figure 30.

An analyzer using this proton calorimetry result for a Resurrection/Titan analysis must decide whether to take the 5% difference as a correction or additional uncertainty.

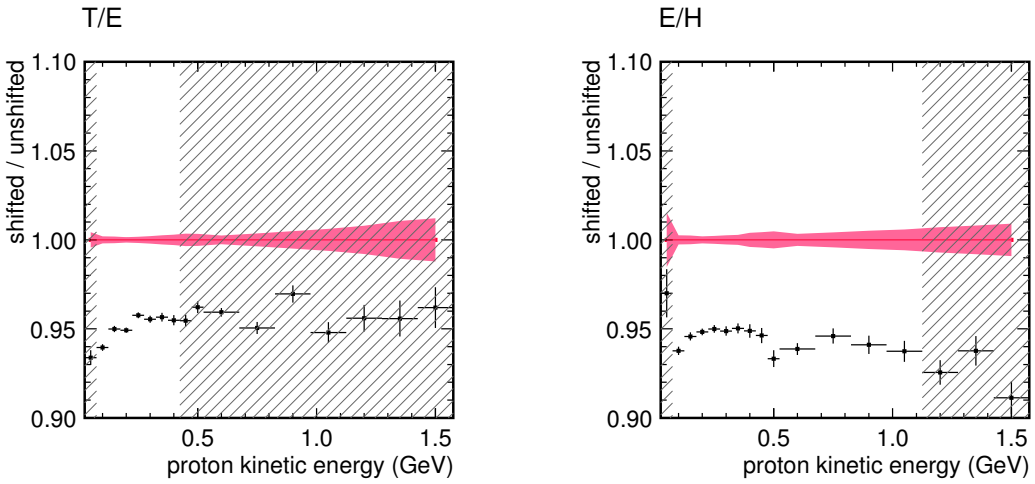

Figure 26: Resurrection-era geometry, hit aggregation, neutron settings and Birks' constant.

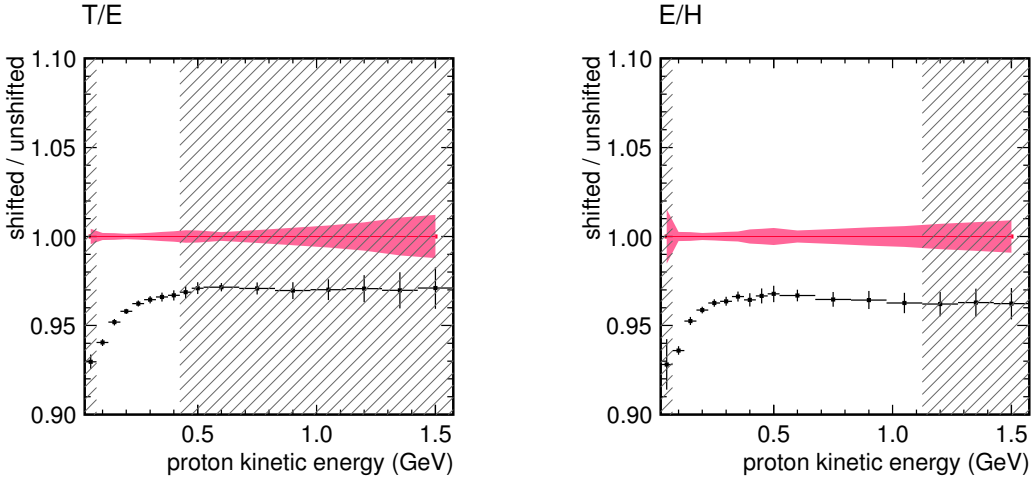

Figure 27: Resurrection-era Birks' constant.

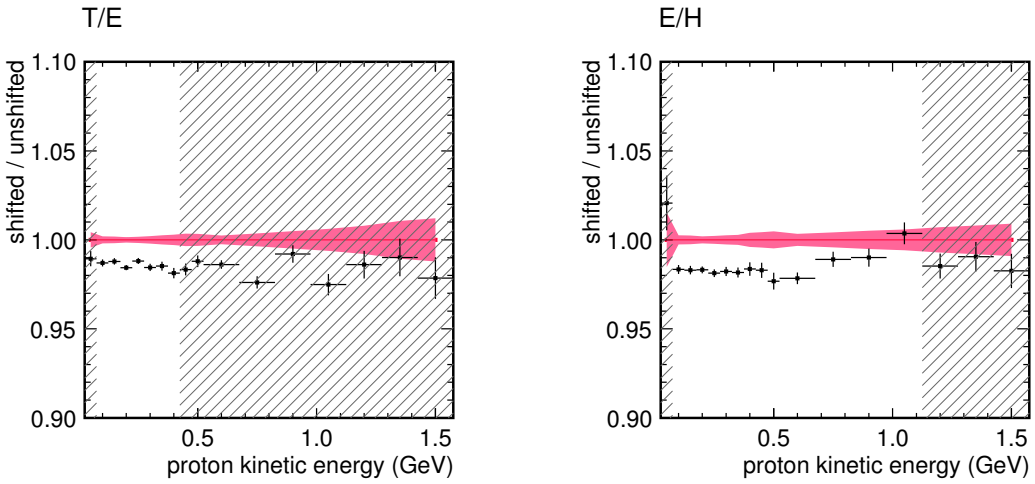

Figure 28: Resurrection-era geometry.

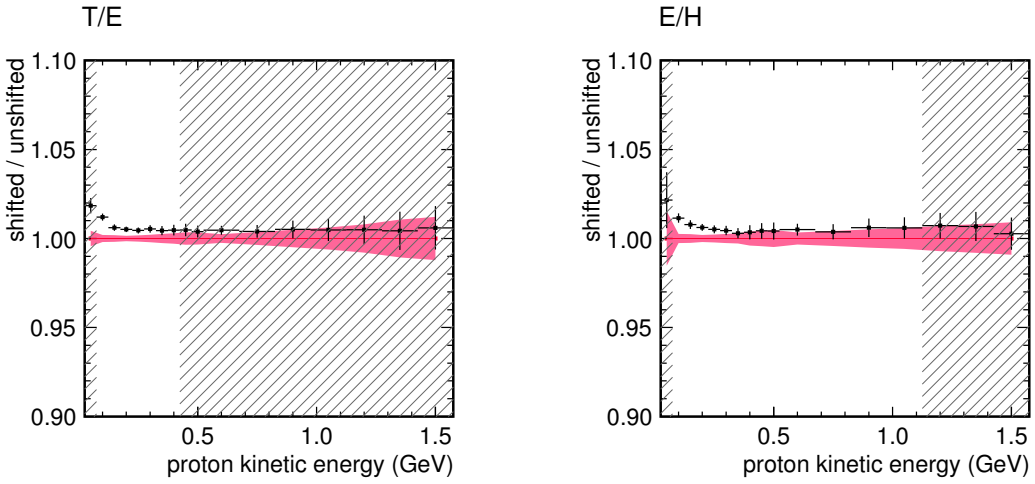

Figure 29: Resurrection-era hit aggregation.

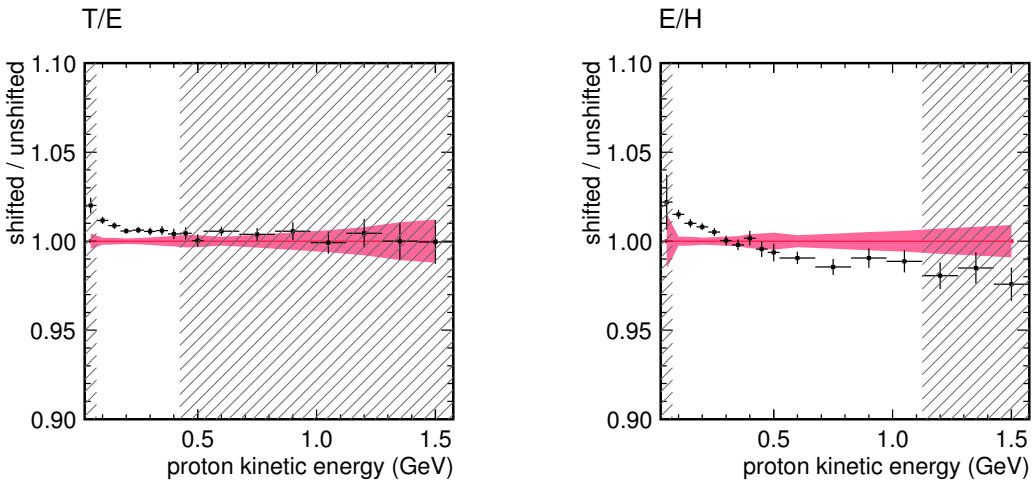

Figure 30: Resurrection-era hit aggregation and neutron settings.

7 Conclusions

Figure 7, the data/MC ratio of mean calorimetric energy / KE, shows the agreement of the calorimetric response of protons to be within systematic errors in the region of good statistics and containment (the unhatched region). The calorimetric energy / KE distributions for the two outlier points, 150 MeV T/E and 900 MeV E/H, are shown in Figure 31. The discrepancy in these bins is evident in the distributions; it is not the result of a few extreme events.

The RMS of the calorimetric energy / KE distribution, shown in Figure 6, is well modeled by the simulation.

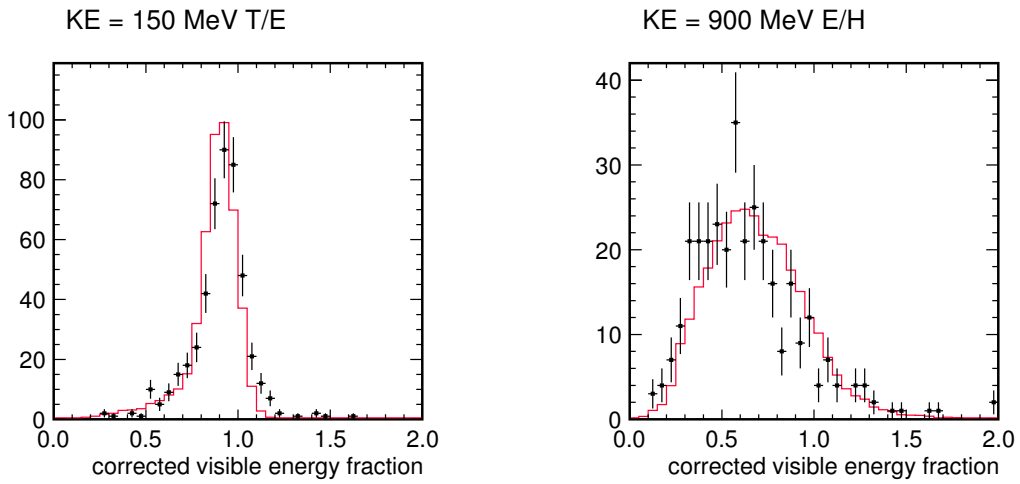

Figure 31: Calorimetric energy / KE for the two outlier bins in the data/MC ratio (Figure 7). **Left:** 150 MeV T/E. **Right:** 900 MeV E/H. Data in black with statistical errors; MC in red.

The two outlier points are ignored, and the final uncertainty on the calorimetric response of protons is taken as the systematic error, 3.0% at the higher kinetic energies. If we feel ambitious, the uncertainty can follow the curve of the systematics band, expanding to 3.5% at 100 MeV. The 50 MeV bin for the T/E detector is shown in Figure 32. The statistical error on the data/MC ratio at this energy is large, but the distributions are convincing. The systematic error at 50 MeV is 4.0%. The same bin for the E/H detector is inconclusive, but a 50 MeV proton in big MINERνA will likely be contained in the tracker region.

Analyzers should take note of the systematic errors included in this result, summarized in Table 1, so as not to double count errors. Birks' constant, for example, is included in the result, and does not need to be explicitly studied for events performing calorimetric reconstruction. For an exclusive state analysis, however, Birks' constant may affect the performance of a selection based on the dE/dx of a stopping proton and must be studied as a systematic.

Three potential systematics should be evaluated separately in big MINERνA:

1. **Cross-talk** – TN018, docdb:8686 has an argument for how cross-talk affects the MEU calibration, repeated in Section 5.1.2. Cross-talk also affects the calorimetric recoil reconstruction, as cross-talk clusters are rejected in the big MINERνA algorithm.
2. **PMT non-linearity** – Though included here, PMT non-linearity may be more of an uncertainty for large showers, particularly with high EM content, in big MINERνA. The simulation currently includes no implementation of PMT non-linearity.

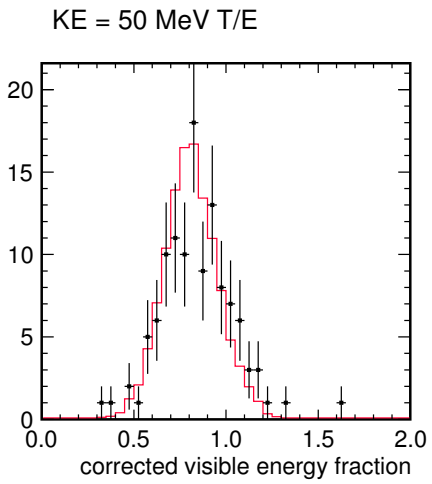

Figure 32: Calorimetric energy / KE for the 50 MeV bin, T/E detector. Data in black with statistical errors; MC in red.

3. **Calorimetry time window** – Section 5.7 shows the effect of including the $(-20, 35)$ ns cut on clusters included in the calorimetric sum. A large effect was observed in test beam protons, but not taken as a systematic uncertainty.

Section 6 explains the differences between the proto-Eroica MC used for test beam analyses and Resurrection/Titan. The differences amount to a 5% higher calorimetric response for protons in the new MC, which can be taken as a correction or additional uncertainty.